Available online at www.sciencedirect.com
ScienceDirect
Catalysis Today 129 (2007) 50–58
CATALYSIS TODAY
www.elsevier.com/locate/cattod

# Hydrothermal preparation of highly photoactive $TiO_2$ nanoparticles

M.C. Hidalgo, M. Aguilar, M. Maicu, J.A. Navío, G. Colón *

*Instituto de Ciencia de Materiales de Sevilla, Centro Mixto, CSIC-Universidad de Sevilla, Américo Vespucio, 49, 41092 Sevilla, Spain*

Available online 31 August 2007

**Abstract**

$TiO_2$ nanoparticles have been prepared by amine assisted sol–gel precipitation of $Ti^{4+}$ aqueous solutions and further hydrothermal treatment. The effect of different starting acidic solution (nitric, chlorhydric and acetic acids) as well as the addition of triethylamine (TEA) at different pH has been widely investigated. It has been stated that different amounts of TEA could have interesting effects upon hydrothermal treatment. Surface and morphological features significantly differ from $TiO_2$ prepared using different synthetic route. In all cases, amine precipitated $TiO_2$ obtained exhibit high conversion values for phenol photo-oxidation reaction, being in certain conditions higher than that exhibited by $TiO_2$ Degussa P25. The precipitation of the acetic acidified solution leads to high surface area values and well crystallized anatase with small crystallite size. In addition, this set of catalysts show the cleanest surface after the hydrothermal treatment. The conjunction of these features would be the characteristic features responsible of the best photocatalytic activity observed.


*Keywords:* $TiO_2$; Triethylamine; Alkoxide; Sol–gel; Hydrothermal; Photocatalysis

## 1. Introduction

It is well established that morphological and structural parameters strongly affect the photocatalytic activity of a semiconductor [1,2]. Titanium dioxide is one of the most important photocatalyst and many works have been devoted to the preparation and modification of this semiconductor [2]. The improvement and optimisation of $TiO_2$ as photocatalyst is an important task for technical applications of heterogeneous photocatalysis in the future.

From the point of view of the enhancement in the efficiencies of the photocatalytic process, it is evident that the tailoring and development of new and alternative photocatalysts can be considered of great interest. The development of new photocatalytic systems goes through the modification in the synthetic process as well as the design of new systems and configurations (nanotubes, mesoporous, thin films, ...) [2]. These modifications in the particular case of $TiO_2$ would lead to: (i) the generation of nanosized particles [3]; (ii) surface modifications improving the charge transfer efficiency or the pollutant adsorption [4]; (iii) ion incorporation (both cationic or anionic) in the $TiO_2$ matrix which could improve the optical absorption properties especially in the visible range [5,6]; (iv) the immobilization of a highly active system [7,8].

The impact of nanostructure on the properties of high surface area materials is an area of increasing importance for understanding, creating and improving materials for diverse applications. A unique property of nanoparticles is their extremely high surface area. The synthesis of nanoparticles with controlled size and composition is of technological interest. As a consequence, there has been a lot of highlighting on the production of nanoparticulated $TiO_2$ for a wide range of applications.

Within this framework, the proposal of new synthetic routes for obtaining highly active $TiO_2$ appears extremely interesting. In this sense, the control of particle size and the use of nanosized semiconductors in photocatalysis has been considered crucial, as already mentioned. Moreover, Wang et al. reported that there is an optimal particle size for photo-oxidation of chloroform on nanocrystalline $TiO_2$ [9,10]. For an intrinsic $TiO_2$ they found it to be around 10 nm. This optimum was attributed to the optimum in surface reaction vs. $e^-/h^+$ recombination.

In the present paper, we report the preparation of highly active $TiO_2$ systems by means of hydrothermal method. In the

* Corresponding author.
*E-mail address:* gcolon@icmse.csic.es (G. Colón).

0920-5861/$ – see front matter © 2007 Published by Elsevier B.V.
doi:10.1016/j.cattod.2007.06.053

literature on hydrothermal synthesis of nanocrystalline titania, the main attention is paid to the hydrothermal treatment of amorphous $TiO_2$ gels [11–13]. In this sense, Kolen'ko et al. [14] reported the effect of the different synthetic parameters on the photocatalytic properties of $TiO_2$. They stated that the structural, electronic and surface properties of $TiO_2$ can be modulated by the adequate hydrothermal conditions. The occurrence of the appropriate features, conditioned by controlling the preparation steps, significantly conditions the *photo* and *catalytic* parts of the photo-oxidation mechanism [14,15].

In our case, we establish interesting correlation between several synthetic parameters and the final photoactivity for phenol degradation. $TiO_2$ gels were obtained by precipitation of a $Ti^{4+}$ aqueous solution using triethylamine (TEA) as precipitating agent. In this sense, it has been reported that the use of amines could act as shape controller template. Thus, secondary amines, such as diethylamine and tertiary amines, such as trimethylamine and triethylamine, acted as a complexing agent of $Ti^{4+}$ ions to promote the growth of ellipsoidal particles of a low aspect ratio [16]. Therefore, different initial acidic $Ti^{4+}$ solutions and the final pH values achieved by addition of TEA were the controlled parameters in the present study.

## 2. Experimental

Different $TiO_2$ series were prepared from initial aqueous $Ti^{4+}$ stock solutions by precipitation by means of different amines and further hydrothermal treatment. These precursor solutions were obtained by adding certain amount of Ti isopropoxide (TTiP)/isopropanol solution (76.7 and 76.4 ml, respectively) to 800 ml of distilled water at pH 1.5 achieved by means of $HNO_3$, HCl or acetic acid (hereafter named as series A, B and C, respectively). After TTiP addition a white precipitate was obtained that upon stirring at room temperature for two days lead to a yellowish homogeneous transparent solution. Different amount of triethylamine (TEA) were then added drop wise to 100 ml of the Ti-solution till pH values reached 7, 9 and 11. The obtained white precipitate suspension (150 ml, which corresponds to 75% of the total reactor volume) was then placed in a Teflon recipient inside of stainless steel autoclave. Hydrothermal treatment was performed at two temperature and time conditions: 120 °C for 24 h and 150 °C for 6 h. At these temperatures, the working pressures are 198.48 and 475.72 kPa, respectively. $TiO_2$ powders were obtained by centrifugation and repeatedly washing (3 times with distilled water). Thus obtained precipitates were then filtered and dried at 120 °C overnight.

Alternatively, calcined set of samples of selected system were obtained by calcination of the amorphous precipitate formed after TEA addition. Thus, after the amine addition, the gels obtained were aged at room temperature for 4 h. Then, after centrifugation, these gels were dried at 120 °C overnight and finally calcined at 400 and 500 °C for 2 h.

BET surface area measurements were carried out by $N_2$ adsorption at 77 K using a Micromeritics 2000 instrument. Pore volumes were determined using the cumulative adsorption of nitrogen by the BJH method.

X-ray diffraction (XRD) patterns were obtained using a Siemens D-501 diffractometer with Ni filter and graphite monochromator. The X-ray source was Cu Kα radiation. From the line broadening of corresponding X-ray diffraction peaks, according to the Warren and Averbach equation (peaks were fitted by using a Voigt function).

$$D = \frac{\lambda\, 180}{\pi \cos\theta\, L}$$

where $L$ is the line width at medium height. λ is the wavelength of the X-ray radiation 0.15406 nm and $\theta$ is the diffracting angle.

Diffuse reflectance spectra were obtained on a UV–vis scanning spectrophotometer Shimadzu AV2101, equipped with an integrating sphere, using $BaSO_4$ as reference. UV–vis spectra were performed in the diffuse reflectance mode ($R$) and transformed to a magnitude proportional to the extinction coefficient ($K$) through the Kubelka–Munk function, $F(R_\infty)$. Band gap values were obtained from the plot of the modified Kubelka–Munk function, $(F(R_\infty)E)^{1/2}$, versus the energy of the absorbed light $E$.

Selected samples were also studied by transmission electron microscopy (TEM) using a Philips CM200 instrument. The microscope was equipped with a top-entry holder and ion pumping system, operating at an accelerating voltage of 200 kV and giving a nominal structural resolution of 0.21 nm. Samples were prepared by dipping a 3 mm holey carbon grid into ultrasonic dispersion of the oxide powder in ethanol.

XPS data were recorded on 4 mm × 4 mm pellets, 0.5 mm thick, prepared by slightly pressing the powdered materials, which were outgassed in the prechamber of the instrument at 150 °C up to a pressure $<2 \times 10^{-8}$ Torr to remove chemisorbed water from their surfaces. The Leibold–Heraeus LHS10 spectrometer main chamber, working at a pressure $<2 \times 10^{-9}$ Torr, was equipped with an EA-200 MCD hemispherical electron analyzer with a dual X-ray source working with Al Ka ($h\nu$ = 1486.6 eV) at 120 W, 30 mA using C (1s) as energy reference (284.6 eV).

Photocatalytic runs (2 h) of phenol oxidation over the different catalysts (1 g/l) were performed in a Pyrex immersion well reactor (450 ml) using a medium pressure 400 W Hg lamp supplied by Applied Photophysics, showing main emission line at 365 nm. In the oxidation tests, an oxygen flow was used to produce a homogenous suspension of the catalyst in the solution. Before each photo-experiment, the catalysts were settled in suspension with the reagent mixture for 15 min in the dark. The evolution of the initial phenol concentration (*ca.* 50 ppm in water) was followed by UV–vis spectrometry through the evolution of its characteristic 270 nm band, using a filtered aliquot *ca.* 2 ml of the suspension (Millipore Millex25 0.45 μm membrane filter). The degradation rates were calculated from the slopes of the conversion plots at the first 15 min of reaction, and assuming a zero order kinetics at this stage of the reaction. The regression coefficients for such fittings are in all cases higher than 0.998.

Table 1
BET surface area and average pore size distribution for $TiO_2$ obtained by different hydrothermal treatment

| Samples | | | 120 °C, 24 h | | | | 150 °C, 6 h | | | |
|---|---|---|---|---|---|---|---|---|---|---|
| Acid type | pH | Name | $S_{BET}$ ($m^2$/g) | Pore diameter (Å) | Anatase molar fraction (%) | Crystallite size (nm) | $S_{BET}$ ($m^2$/g) | Pore diameter (Å) | Anatase molar fraction (%) | Crystallite size (nm) |
| $HNO_3$ Series A | 11 | A1 | 180 | 46 | 86 | 7 | 178 | 45 | 78 | 6 |
| | 9 | A2 | 196 | 45 | 84 | 6 | 191 | 50 | 78 | 5 |
| | 7 | A3 | 204 | 44 | 88 | 6 | 216 | 50 | 76 | 5 |
| | 1.5 | A0 | 190 | 38 | 64 | 5 | 246 | 40 | 86 | 4 |
| HCl Series B | 11 | B1 | 182 | 45 | 82 | 7 | 157 | 70 | 60 | 5 |
| | 9 | B2 | 172 | 50 | 68 | 5 | 202 | 45 | 91 | 6 |
| | 7 | B3 | 183 | 45 | 55 | 5 | 215 | 50 | 65 | 5 |
| | 1.5 | B0 | 89 | 250 | 14 | 5 | 183 | 30 | 70 | 5 |
| HAc Series C | 11 | C1 | 114 | 101 | 100 | 11 | 139 | 70 | 100 | 10 |
| | 9 | C2 | 132 | 70 | 100 | 10 | 150 | 70 | 100 | 9 |
| | 7 | C3 | 193 | 45 | 100 | 7 | 202 | 70 | 100 | 9 |
| | 1.5 | C0 | 194 | 52 | 100 | 9 | 221 | 65 | 100 | 10 |

## 3. Results and discussion

Surface data corresponding to the resulting samples from both hydrothermal treatments are summarized in Table 1. In general, hydrothermal treatment leads to high surface area values, as it has been widely reported in literature for hydrothermal synthesis [14,17]. Thus, all photocatalysts present higher surface area with respect to similar $TiO_2$ systems prepared in our group by typical sol–gel and further calcination procedure [4,18]. Systems prepared by using different acids show surface area values in the range of 150–250 $m^2$/g depending on hydrothermal conditions and the final pH of the $Ti^{4+}$ solution. It is worthy to note that as TEA is added, and pH values increase, it seems that a slight diminution in $S_{BET}$ value is observed in all systems. Furthermore, preparation at higher temperature, that is 150 °C for 6 h, does not produce significant differences with respect surface area values and similar trend is observed within each series of samples as pH varies (Table 1).

Pore size distribution corresponding to series A, B and C obtained by means of both hydrothermal treatments is shown in Fig. 1. From these plots, the average pore sizes for series A and B ranged between 40 and 60 Å, independently of the hydrothermal treatment submitted. In addition, in each series the precipitation at different pH values do not induce to any significant differences in the pore distribution. Only in the particular case of B, sample prepared in the absence of the amine (B0), the pore distribution appears completely different

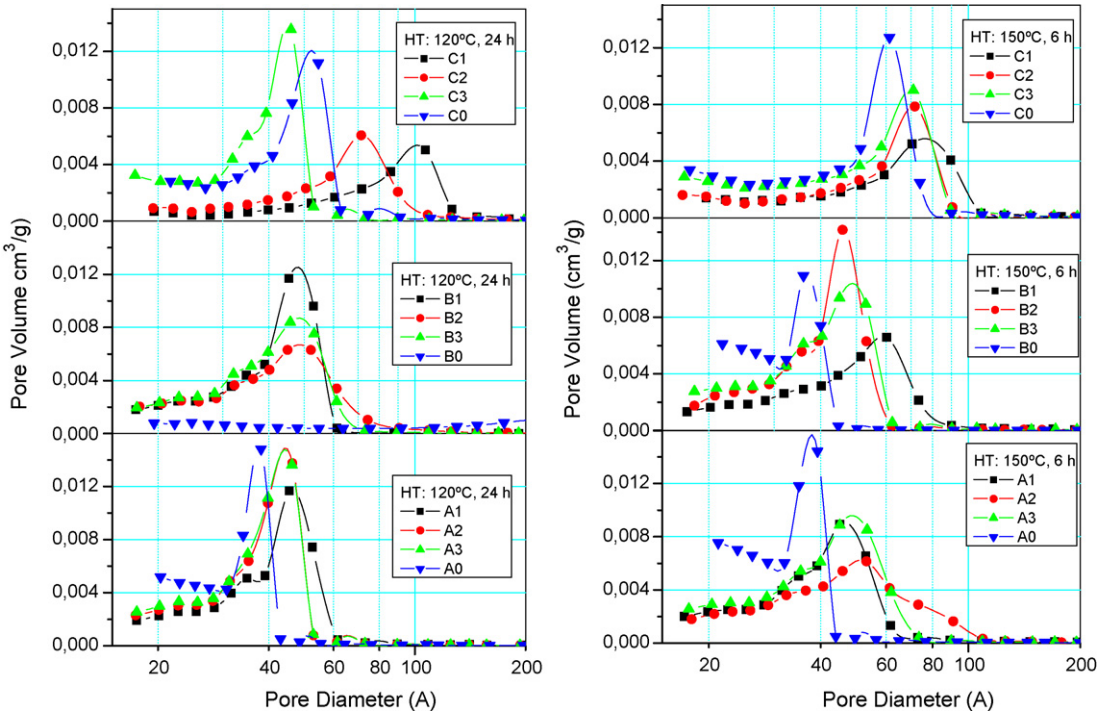


Fig. 1. Average pore size distribution for different $TiO_2$ samples.

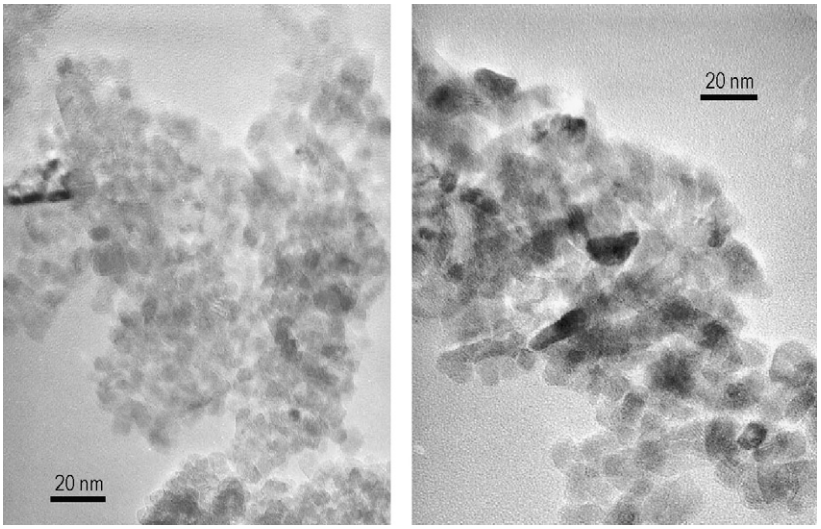


Fig. 2. Selected TEM images for A1 (left) and C1 (right) $TiO_2$ samples.

with respect to the rest showed in Fig. 1. A similar singularity was also appreciated in the BET surface area for this sample, being appreciably lower than the rest. On the contrary, series C presents a certain evolution in the average pore size with the pH of precipitation with TEA. Thus, as precipitation pH arises, the average pore size appears shifted towards higher values. Sample C obtained upon precipitation at higher pH (pH 11), that is C1 sample, exhibits an average pore size of 100 Å, in contrast with the 50 Å exhibited by C0. Hydrothermal treatment at higher temperature (Fig. 1) produces a similar evolution in the pore size distribution. Thus, series A and B exhibit no clear pH dependence and series C keep the observed evolution with pH values, though in this case, the pore size growth appears smoothed with respect to lower temperature synthesis.

The different synthesis studies also produces significant differences under the structural point of view (Table 1). Hydrothermal synthesis at 120 °C for 24 h, leads to mainly anatase structure in all systems independently of the pH value. Only in the case of B, sample prepared in the absence of the amine (B0 sample), rutile is the main crystalline phase present. Systems A and B exhibit small rutile fraction, in addition to anatase one, being more evident this rutile phase for B system. Regarding to these two series, it is noticeable that meanwhile for A series, the anatase fraction is similar for different precipitation pH values, B series shows a slight dependence with pH and rutile phase fraction decays for higher pH values. On the contrary, C system appears only in the anatase phase with higher crystallinity with respect to A and B. Hydrothermal synthesis at 150 °C for 6 h, induces similar structural features.

The evolution of crystallite size measured from XRD pattern peak broadening is reported in Table 1. For hydrothermally treated samples at 120 °C, the general trend in crystallite size clearly indicates a slight growth as pH value increases for all systems. In this sense, crystallinity of anatase phase seems to be similar for series A and B. While for C systems, mean crystallite sizes are slightly higher than the first, as it was previously stated, and exhibit a considerable growth with pH increasing. On the other hand, treatment at 150 °C produces similar differences between A, B and C series. In this case, pH values do not seem to have any influence in the crystallite size for amine precipitated powders. From the structural point of view, it is clear that series A and B clearly differs from series C. Thus, A and B series exhibit mean crystallite size for anatase of 5–6 nm, exhibiting small rutile fraction; while C series presents only anatase phase with crystallite size around 10 nm.

In Fig. 2, we show the comparison of TEM images corresponding to A1 and C1 samples. TEM images clearly illustrate the particle sizes for selected samples, which is in agreement with calculated values from XRD. Therefore, in both hydrothermal treatments small crystallite size materials are obtained, with values raging between 5 and 10 nm. In both cases, rather aggregated rounded particles are found, and this is representative of all samples studied. It is also noticeable that C1 particles clearly appear with a slight higher crystallite size and better defined than those observed for A1, which is in accordance with XRD data.

Regarding to the optical absorption properties, the UV–vis diffuse reflectance spectra (not shown) are in good agreement with the structural evolutions mentioned before. All systems show similar absorption spectra with absorption edges around 400 nm. Band gap values calculated from these plots ranged between 3.15 and 3.50 eV. The small differences found in the band gap values can be attributed to crystallite size and the different crystal phase (rutile in the case of B series), as described in previous section. Thus, the preparation using TEA as precipitating agent does not lead to any modification in the absorption spectra of these systems though some authors described the incorporation of nitrogen by precipitation using ammonia or other amine systems [5,19,20]. So in principle, we might infer that this incorporation effect has not taken place in our systems and amine only would act as precipitating agent that could complex in certain way to $Ti^{4+}$ precursor.

We have performed XPS analysis of selected samples, which will provide us useful information about the situation of the photocatalysts surface. The observed binding energy values for

Table 2
XPS analysis for different $TiO_2$ samples prepared from hydrothermal method

| Acid type | pH | HT 120 °C, 24 h | | | HT 150 °C, 6 h | | |
|---|---|---|---|---|---|---|---|
| | | N (at.%) | C (at.%) | O/Ti ratio | N (at.%) | C (at.%) | O/Ti ratio |
| $HNO_3$ | 11 | 0.68 | 8.59 | 2.02 | 0.70 | 10.14 | 1.92 |
| | 1.5 | 0.65 | 16.26 | 2.21 | 0.52 | 13.63 | 2.06 |
| HCl | 11 | 0.58 | 14.31 | 2.17 | 0.53 | 12.78 | 2.12 |
| | 1.5 | 0.79 | 12.86 | 2.06 | 0.35 | 8.45 | 2.02 |
| HAc | 11 | – | 7.66 | 2.02 | – | 8.62 | 2.05 |
| | 1.5 | – | 10.35 | 2.12 | – | 9.76 | 2.17 |

Ti (2p) and O (1s) are located at 485.5 and 530.0 eV, respectively, being the typical values reported for $TiO_2$ [4]. For the O (1s) peak, an additional small shoulder located at 531 eV denotes the presence of surface OH groups (not shown). This contribution is similar for all systems, indicating similar hydroxylated surface in all cases.

XPS data also indicate us the presence of adsorbed species from the precipitation solution, not eliminated in the washing procedure (Table 2). In this sense, it is worthy to note the presence of C and N probably coming from the amine used in the precipitation process remaining after washing step. In addition, for B0 sample a small amount of chlorine is found,

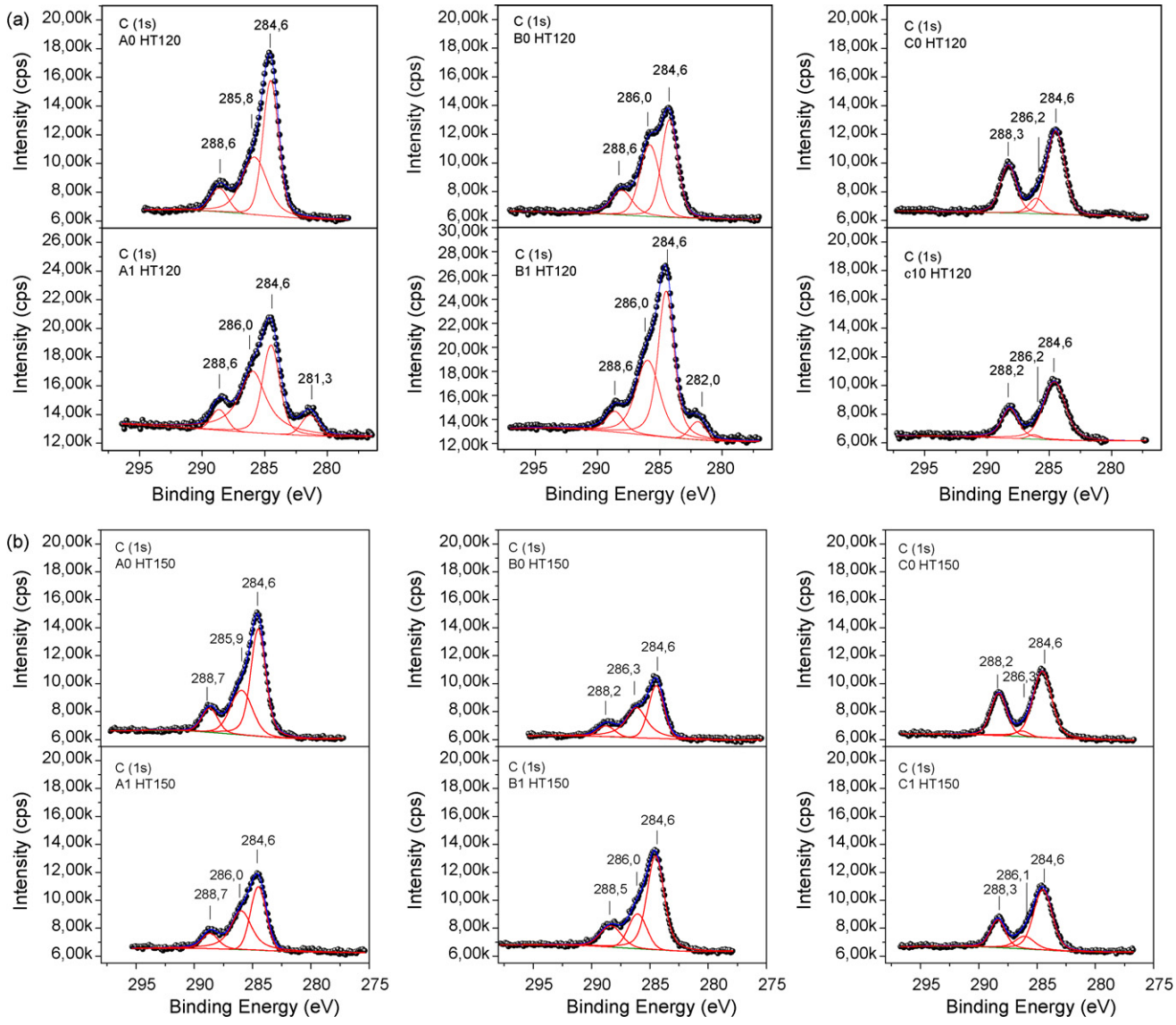


Fig. 3. XPS spectra for C (1s) level corresponding to (a) $TiO_2$ series prepared at 120 °C for 24 h and (b) $TiO_2$ series prepared at 150 °C for 6 h.

presumably from the HCl acid used in the stock $Ti^{4+}$ solution. The presence of Cl species at the surface could explain the particularities in the structural and surface features of this sample previously mentioned. The amount of nitrogen is in any case significantly low (around 0.5 at.%) and as it has been stated, do not lead to any changes in the absorption spectra. Therefore, we may infer from these results that the nature of this adsorbed nitrogen could be related to adsorbed species instead of structurally substituted one. The relative amount of *N*-species might be considered negligible since samples obtained without amine precipitation also show certain nitrogen at the surface, probably due to atmospheric contamination. In any case, it is remarkably that for C series the N present at the surface seems to be lower than in the case of A and B series. The position of N (1s) peak around 400 eV clearly indicates that the nature of the nitrogen present at the surface would corresponds to NO or NH species, or even to molecular chemisorbed $\gamma$-$N_2$, in contrast to the reported binding energy of 396 eV assigned to Ti–N bond [19,21,22].

In addition, it is also noticeable the significant amount of carbon in all systems, probably coming from the organic precursors used. As in the case of nitrogen, the presence of carbon is more important in series A and B. Therefore, the occurrence of both species (C and N) might be related to the existence of adsorbed organic species from Ti-alkoxide precursor and TEA. The preparation in different acid media leads to different surface situation in the precipitate. It seems that only in the case of acetic acid (series C) the organic species are less retained at the surface and therefore final powder appears with a cleaner surface (see Table 2).

If we study the XPS spectra for C (1s) level (Fig. 3), it is clear that the surface situation with respect to carbon species is completely different among A, B and C series. From deconvolution of C (1s) band, in all cases, several carbon species might be considered. Thus, the peaks located around 288.6, 286.0 and 284.6 eV indicate the presence of different carbonaceous species adsorbed at the surface. These different peaks could be attributed to C–C, C–O, C=O and O–C=O bonds [23]. Same carbonaceous species are found for two set of samples obtained by means of different hydrothermal treatments. In both set of samples, a noteworthy difference can be drawn among A, B and C series. Thus, meanwhile A and B samples exhibit similar C (1s) spectra, C series presented a rather unlike one. For these later series, the C (1s) spectra show strong peaks around 288 and 284.6 eV. A large diminution in the peak located *ca.* 286 eV together with a slight increase in

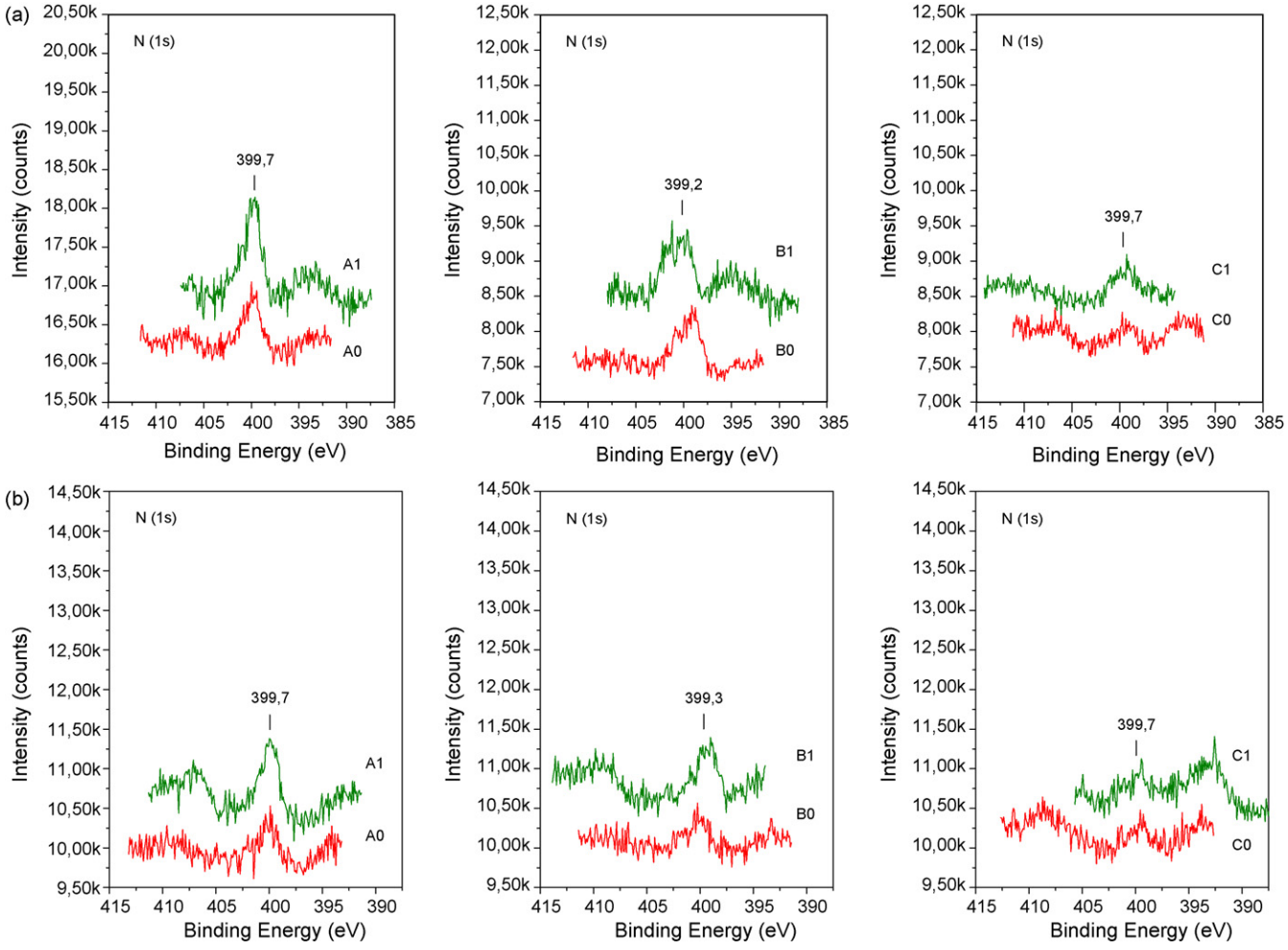


Fig. 4. XPS spectra for N (1s) level corresponding to (a) $TiO_2$ series prepared at 120 °C for 24 h and (b) $TiO_2$ series prepared at 150 °C for 6 h.

the 288 eV peak is observed for C series. Thus, C series presents lower carbon content probably due somewhat to the diminution in the species associated to 286 eV contribution in the C (1s) spectrum.

In Fig. 4, we show the XPS spectra corresponding to the N (1s) level for $TiO_2$ prepared by both hydrothermal methods. As we have observed from Table 2, both treatments lead to similar nitrogen content. However series C clearly exhibit lower N (1s) bands, practically negligible. On the other hand, from the position of the peak, located around 399–402 eV, it is clear that the nature of this nitrogen species can be associated to adsorbed nitrogen impurities coming from nitrate, in the case of A series, and –NH rests from TEA [19,21,22]. This binding energy value, do not correspond to the value reported in the literature assigned to structurally substituted nitrogen into the $TiO_2$ matrix [20]. So, we can consider that this small amount of surface nitrogen might be associated to nitrogen impurities from the preparation procedure as well as atmospheric contamination.

Photocatalytic activity of the different series of $TiO_2$ is summarized in Fig. 5. The first feature that can be inferred is that the reaction rates for systems prepared by hydrothermal treatment at 120 °C for 24 h appear noticeable higher than those exhibited by samples prepared at 150 °C for 6 h. In addition, it is clear that for this set of systems, the precipitation in the presence of TEA visibly enhance the photocatalytic activity of all series. Within this set of systems, series C shows a remarkably higher reaction rates with respect to A and B series. In this sense, it is worthy to note that C1 and C2 (samples prepared at pH 11 and 9, respectively), present the highest values within its series, being even higher than that obtained for $TiO_2$ Degussa P25. On the other hand, set of systems prepared at 150 °C presents a diminution in the reaction rates, especially for samples precipitated in the presence of TEA. Thus, within this set, samples A0, B0 and C0 appear with comparable reaction rates with respect to those precipitated at alkaline pH values with TEA.

In order to explain the enhancement of the hydrothermal treatment, we have also studied the photocatalytic behaviour of fresh C1 photocatalyst calcined at 400 and 500 °C for 2 h. The surface and structural characterisation data for these calcined samples are summarised in Table 3. As it can be observed from this table, in both cases only anatase structure is obtained. However and as expected, surface area values for these calcined samples appear lower than in the case of samples prepared by hydrothermal synthesis. The conversion plot for these two samples is shown in Fig. 6. These calcined systems show similar photocatalytic activities (see Table 3) and in any case with lower efficiencies with respect hydrothermally treated one (Fig. 5). Thus, from this direct comparison, it can be inferred that hydrothermal treatment leads to higher active systems with respect to calcined ones. In principle, the remarkably surface area diminution could be responsible of the lower reaction rates observed for these samples (Table 3).

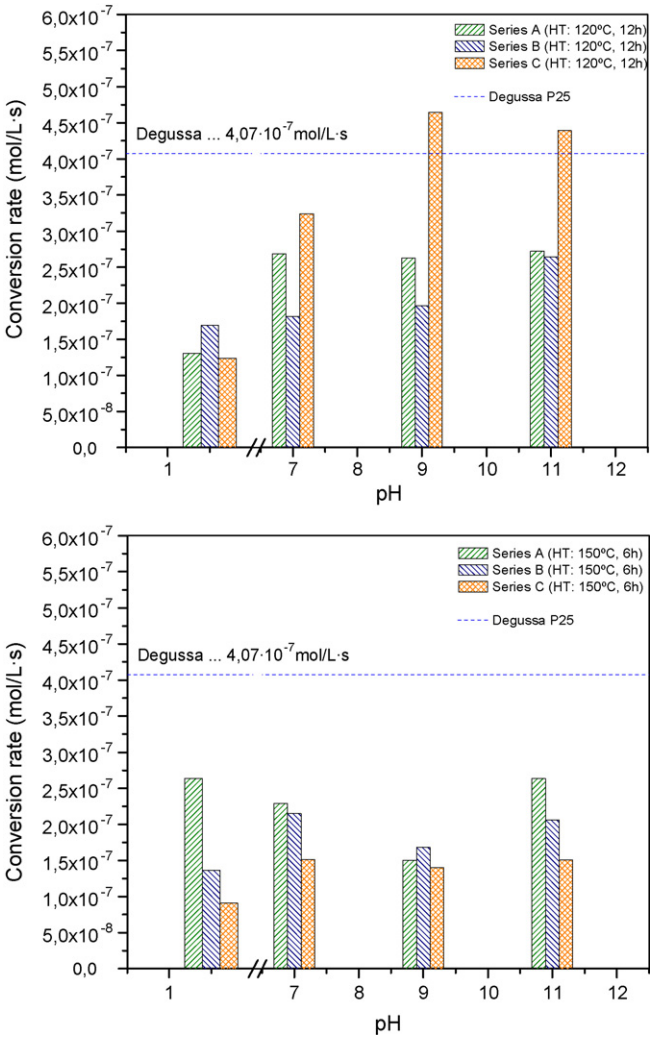


Fig. 5. Photocatalytic activity for phenol degradation corresponding to different $TiO_2$ samples.

As previously stated, the high surface area values obtained for hydrothermally treated samples could explain the important photoactivities of these samples. In this sense, it would be interesting to establish the surface area influence on the photocatalytic activity for the studied systems. For this reason, we have plotted the conversion rate per surface area unit (Fig. 7). From this figure, it is clear that for most of the hydrothermally prepared systems, the conversion rates appear similar, with a clear exception for C series precipitated in the presence of TEA and treated at 120 °C. That means that surface area values are not responsible of the high difference in

Table 3
Surface and structural features for $TiO_2$ C1 systems obtained by calcination at different temperature

| Sample | | $S_{BET}$ ($m^2$/g) | Average pore diameter (Å) | Anatase molar fraction (%) | Crystallite size (nm) | Reaction rate (mol/l s) |
|---|---|---|---|---|---|---|
| Fresh C1 | 400 °C | 114 | 75 | 100 | 12 | $1.8 \times 10^{-7}$ |
| | 500 °C | 68 | 70 | 100 | 16 | $1.6 \times 10^{-7}$ |

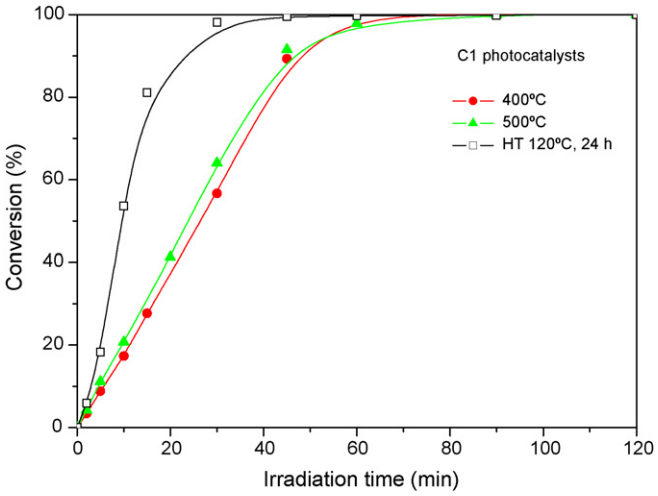


Fig. 6. Comparison between the photocatalytic conversion plots corresponding to hydrothermal and calcined C1 systems.

reactivities observed in Fig. 5. On the other hand, the specific rates are also higher than in the case of calcined C1 systems, which exhibit significantly lower surface area. Thus, for equal surface area of catalyst considered C1 series exhibit higher photoactivity for phenol degradation. Therefore, the explanation for this particular behaviour might be looked by considering other structural features observed for these series, particularly different from A and B series. The occurrence of well crystallized anatase with small crystallite sizes (*ca.* 10 nm) and a cleaner surface should be the reasons for the specific photocatalytic activity. These structural and surface features would favour the complex photocatalytic mechanism, involving both *photo* and *catalytic* considerations [14]. In spite of this performed efficiency of this C series, $TiO_2$ Degussa P25 visibly shows the best specific photoactivity, revealing better structural situation for the photocatalytic process. Probably, the presence of certain amount of rutile phase in the particular structural configuration of Degussa would lead to this

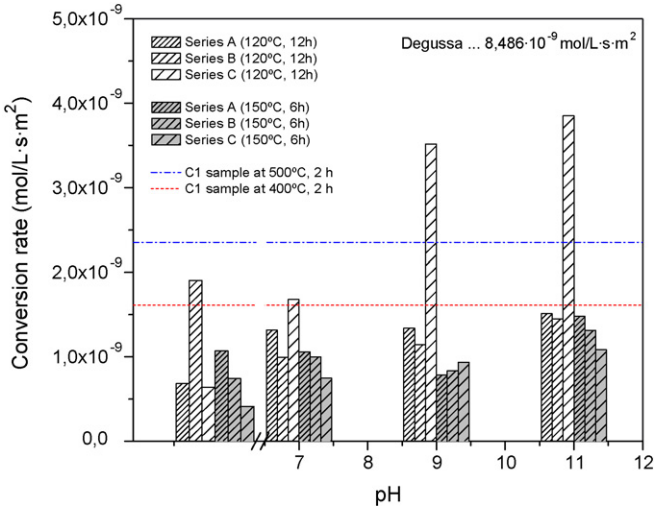


Fig. 7. Specific photocatalytic activity for phenol degradation corresponding to different $TiO_2$ samples.

significantly higher specific photoactivity value referred to the surface area.

## 4. Conclusions

We have obtained a highly active $TiO_2$ prepared from amine precipitation of $Ti^{4+}$ aqueous solution and further hydrothermal treatment. Photocatalytic behaviour of series obtained at the highest temperature hydrothermal treatment produces a general diminution in the photocatalytic activity. Best photocatalytic results were achieved by using C series catalysts after hydrothermal treatment at 120 °C for 24 h. At these hydrothermal conditions, the precipitation pH also has a significant effect on the reactivity of $TiO_2$. Thus, for series C, it appears that as precipitation pH increases, the reaction rate is also enhanced. On the contrary, no clear effect of pH was observed for series obtained at 150 °C for 6 h. Regarding to the kind of acid used in the initial aqueous $Ti^{4+}$ solution, catalysts obtained from acetic acid solution exhibit the best photocatalytic behaviour, having reaction rates even higher than Degussa P25.

From the surface and structural characterization performed, it can be inferred that C series presents well crystallized anatase structure with low crystallite size (*ca.* 10 nm), with high surface area values and the cleanest surface situation after hydrothermal treatment. The conjunction of all these features would lead to highly active $TiO_2$ anatase particles. This high photoactivity is explained by considering an improvement in the different steps in the photocatalytic mechanism, though taking apart the surface area contribution the best photocatalyst in our series do not reach the specific rate exhibited by Degussa P25. Thus, the structural features affecting to the electronic transfer and diffusion of charge carriers might be improved in order to compete with Degussa photocatalyst.

## Acknowledgements

Financial support from project CTQ2004-05734-C02-02 and P.A.I. group project reference FQM181 are acknowledged. Ms. M. Aguilar thanks her Introduction to Research Fellowship by CSIC. Dr. M.C. Hidalgo thanks the Spanish ''Ministerio de Educación y Ciencia'' for her *Ramón y Cajal* Programme Project no. 2003/1116.

## References

[1] G. Colón, C. Belver, M. Fernández-García, Nanostructured oxides in photocatalysis, in: M. Fernández-García, J.A. Rodríguez (Eds.), Synthesis, Properties and Application of Oxide Nanoparticles, Wiley, USA, 2007, Chapter 17, ISBN: 978-0-471-72405-6.
[2] O. Carp, C.L. Huisman, A. Reller, Prog. Solid State Chem. 32 (2004) 33.
[3] M. Tomkiewicz, Catal. Today 58 (2000) 115.
[4] G. Colón, M.C. Hidalgo, G. Munuera, I. Ferino, M.G. Cutrufello, J.A. Navío, Appl. Catal. B: Environ. 63 (2006) 45.
[5] R. Asahi, T. Morikawa, T. Ohwaki, K. Auki, Y. Taga, Science 293 (2001) 269.
[6] A. Fuerte, M.D. Hernández-Alonso, A.J. Maira, A. Martínez-Arias, M. Fernández-García, J.C. Conesa, J. Soria, G. Munuera, J. Catal. 212 (2002) 1.

[7] M.C. Hidalgo, S. Sakthivel, D. Bahnemann, Appl. Catal. A: Gen. 277 (2004) 183.
[8] M.C. Hidalgo, D. Bahnemann, Appl. Catal. B: Environ. 61 (2005) 259.
[9] C.C. Wang, Z. Zhang, J.Y. Ying, Nanostruct. Mater. 9 (1997) 583.
[10] Z. Zhung, C.C. Wang, R. Zakaria, J.Y. Ying, J. Phys. Chem. B 102 (1998) 10871.
[11] K. Yanagisava, Y. Yamamoto, Q. Feng, N. Yamasaki, J. Mater. Res. 13 (1998) 825.
[12] C.C. Wang, J.Y. Ying, Chem. Mater. 11 (1999) 3113.
[13] K. Yu, J. Zhao, Y. Guo, X. Ding, H. Bala, Y. Liu, Z. Wang, Mater. Lett. 59 (2005) 2515.
[14] Yu.V. Kolen'ko, B.R. Churagulov, M.J. Kunst, L. Mazerolles, C. Colbeau-Justin, Appl. Catal. B: Environ. 54 (2004) 51.
[15] S. Boujday, F. Wünsch, P. Portes, J.F. Bocquet, C. Colbeau-Justin, Sol. Energy Mater. Sol. Cells 83 (2004) 421.
[16] T. Sugimoto, X. Zhou, A. Muramatsu, J. Colloid Interface Sci. 259 (2003) 53.
[17] H. Kominami, J. Kato, Y. Takada, Y. Doushi, B. Ohtani, S. Nishimoto, M. Inoue, T. Inui, Y. Kera, Catal. Lett. 46 (1997) 235.
[18] G. Colón, J.M. Sánchez-España, M.C. Hidalgo, J.A. Navío, J. Photochem. Photobiol. A: Chem. 179 (2006) 20.
[19] J.C. Hong, C.V. Bang, D.H. Shin, H.S. Uhm, Chem. Phys. Lett. 413 (2005) 454.
[20] X. Chen, Y. Lou, A.C.S. Samia, C. Burda, L. Gole, Adv. Funct. Mater. 15 (2005) 41.
[21] Y. Nosaka, M. Matsushita, J. Nishino, A.Y. Nosaka, Sci. Technol. Adv. Mater. 6 (2005) 143.
[22] Z. Wang, W. Cai, X. Hong, X. Zhao, F. Xu, C. Cai, Appl. Catal. B: Environ. 57 (2005) 223.
[23] A. Derylo-Marczewska, A. Swiatkoski, B. Buczek, S. Biniak, Fuel 85 (2006) 410.